Nonlocal Mechanism of Self-Organization and Centering of Microtubule Asters

E. N. Cytrynbaum[a], V. Rodionov[b], A. Mogilner[c,*]

[a] *Department of Mathematics, University of British Columbia, Vancouver, BC, Canada V6T 1Z2*
[b] *Department of Physiology and Center for Biomedical Imaging Technology, University of Connecticut Health Center, Farmington, CT 06032, USA*
[c] *Department of Mathematics and Center for Genetics and Development, University of California, Davis, CA 95616, USA*

Abstract Fragments of fish melanophore cells can form and center aggregates of pigment granules by dynein-motor-driven transport along a self-organized radial array of microtubules (MTs). We present a quantitative model that describes pigment aggregation and MT-aster self-organization and the subsequent centering of both structures. The model is based on the observations that MTs are immobile and treadmill, while dynein-motor-covered granules have the ability to nucleate MTs. From assumptions based on experimental observations, we derive partial integro-differential equations describing the coupled granule–MT interaction. We use scaling arguments and perturbation theory to study the model in two limiting cases. The model analysis explains the mechanism of aster self-organization as a positive feedback loop between motor aggregation at the MT minus ends and MT nucleation by motors. Furthermore, the centering mechanism is explained by the spontaneous nucleation of MTs throughout the cytosol which acts as a volume sensing tool. Numerical simulations lend additional support to the analysis. The model sheds light on role of polymer dynamics and polymer–motor interactions in cytoskeletal organization.

---

*Corresponding author.
E-mail address:* mogilner@math.ucdavis.edu (A. Mogilner).

1. Introduction

Many fish and amphibia are able to change skin color rapidly for camouflage or to establish dominance. These changes are possible due to the transport of small organelles, referred to here as pigment granules, within specialized cells called melanophores. The change in color of these cells is derived from transport of the granules to and from the cell center (Bray, 2002; Nascimento et al., 2003). When the pigment is dispersed throughout the cytoplasm, it absorbs light, and the cell appears colored. When the granules aggregate at the center, most of the cytoplasm is transparent to light, and the cell appears colorless.

Within each melanophore, thousands of pigment granules are transported during these color changes. This movement relies on the association of the granules with multiple molecular motors that are able to transduce the chemical energy of ATP hydrolysis into mechanical force generation and movement (Bray, 2002). These motors transport the granules along two kinds of linear polymers—actin and microtubules (MTs) that are organized into a cytoskeleton meshwork that determines cell shape and is required for movement (Bray, 2002). Both kinds of polymers are polar, with so-called minus ends and plus ends displaying distinct structure and kinetics. One important type of dynamic behavior, when the rates of polymer subunit assembly onto the plus ends and disassembly from the minus ends are equal, is called treadmilling. A treadmilling polymer translocates in space in the direction of its plus end despite the fact that the subunits embedded in the polymer remain fixed in space. The movement is rather due to the diffusion in the cytoplasm of the subunits disassembling from the minus end and assembling onto the plus end.

While actin polymers are short, disordered and responsible for the dispersion of the granules, MTs are long and ordered into the radial array called a MT aster (Kellogg et al., 1994), in which the minus ends are focussed at the cell center and plus ends extend outward to the cell boundary (Fig. 1). This structure is crucial for pigment aggregation at the cell center, because some of the motor molecules coating the granules are cytoplasmic dynein motors which, when activated, glide toward MT minus ends (Holzbaur and Vallee, 1994).

MT aster formation is normally attributed to the capacity of the specialized organelles—centrosomes—to nucleate and stabilize the MT minus ends (Schiebel, 2000). The central position of the centrosome is actively maintained in living cells, and recent work indicates that an important role in this centering is played by forces generated by molecular motors and MT polymerization (Burakov et al., 2003). However, remarkably, polar MT arrays can self-organize and center in the absence of centrosomes (Verde et al., 1991; Nedelec et al., 1997). The model of aster formation suggested in (Verde et al., 1991) is based on the ability of multivalent minus-end directed motor complexes to associate with two or more MTs simultaneously and to stay attached to a MT upon reaching its minus end. The model asserts that MT minus-end focusing is achieved by the simultaneous motor driven transport of each MT to the minus ends of the other MTs attached to the same motor complex. Centering can be explained by the balance of length-dependent MT buckling forces which is achieved when the focal point of the MT aster is at the center (Nedelec et al., 1997; Tran et al., 2001). These studies
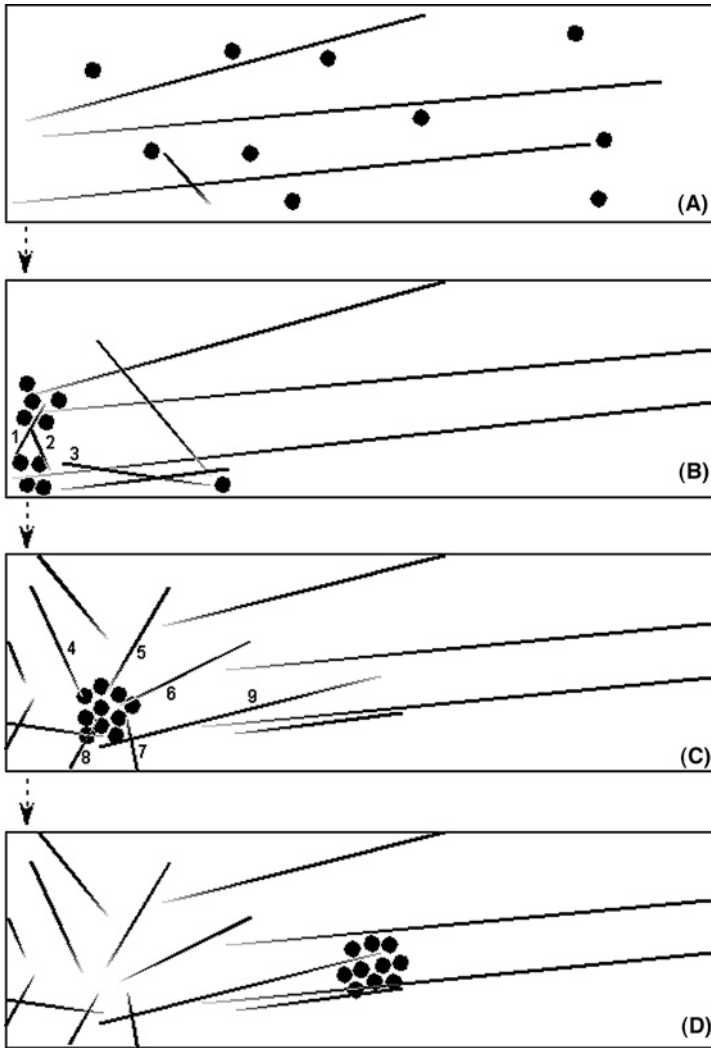
Fig. 1 (A–D) Qualitative model of the granule aggregation, MT aster self-organization and centering. In the nascent fragment, initially (A) the granules are scattered throughout the fragment, while MTs (shown with light minus and dark plus ends) are polarized. First, the motors transport the granules toward a few minus ends, and the granule clusters nucleate MTs (1, 2, 3) the plus ends of which grow and reach other clusters (B). These MTs serve as tracks to merge all clusters into a single aggregate. This aggregate nucleate many MTs (4–8) that start to grow into a MT aster (C). However, rare spontaneously nucleated MTs (9) shift the whole granule aggregate toward the center of the fragment (D). (E–F) Experimental observation of the aggregate centering in the nascent fragment. Within 1 min, the granule aggregate is formed near the edge of the fragment cut off from the cell (E). In 10–15 min, the aggregate moves to the center of the fragment (F). The spatial scale is on the order of tens of microns. Tissue cultures of black tetra melanophores were prepared as described in (Rodionov et al., 1994). To prepare fragments, melanophore processes were dissected with microneedles with a 0.1 μm tip diameter. Aggregation of granules in the fragments was triggered with 0.5 μM adrenalin. Phase contrast images of fragments were obtained using a Nikon TE300 microscope equipped with a Watek high-resolution video camera.
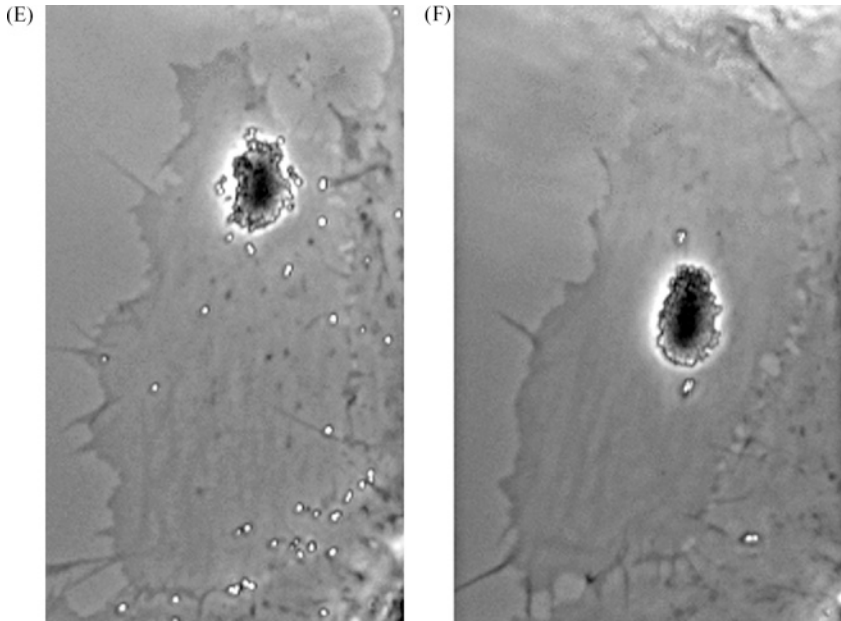
Fig. 1 Continued

emphasized the role of the physical movement of MTs and active force generation by MT elastic bending as opposed to the view of MTs as immobile tracks.

In this paper, we analyze experiments in the model system—microsurgically produced cytoplasmic fragments of fish melanophores. This model system is similar to an intact melanophore in every aspect except for the lack of a centrosome and a pre-centered radial array of MTs but nonetheless, upon motor stimulation, rapidly forms such an array along with an aggregate of pigment granules. These experiments (Rodionov and Borisy, 1997; Vorobjev et al., 2001) demonstrated that when dynein motors are activated in *incubated* fragments with uniformly distributed pigment granules and a random disordered MT array, the MTs rapidly rearrange into an aster with pigment granules and MT minus ends focussed at the center and plus ends at the fragment boundary. Also, in *nascent* fragments with uniformly distributed pigment granules but MTs pre-organized by the centrosome of the mother cell, the granules rapidly aggregate to the edge of the fragment where the minus ends are concentrated. The aggregate subsequently shifts to the center of the fragment (Fig. 1E–F).

The experiments with melanophore fragments suggest a different model of MT aster formation than the multivalent motor transport model (Verde et al., 1991; Nedelec et al., 1997) because recent studies showed that MTs are *not transported* through the cytoplasm (Vorobjev et al., 2001) but simply treadmill. Therefore, melanophore fragments provide a simple and specialized experimental system for studying a form of MT/motor self-organization that relies on the traditional view of MTs as immobile tracks. Previously, we (Cytrynbaum et al., 2004; Malikov et al., 2005) and others (Maly and Borisy, 2002) introduced models of the

self-organization and centering similar to the one considered here, but focussed on numerical and computational, rather than on analytical treatment. In this paper, we derive a modified mathematical model of the phenomenon and use scaling arguments, perturbation theory and numerical analysis to obtain results that lend further insight into the cell behavior. In the next section, we discuss assumptions and derive the model equations. Then, we use scaling arguments and perturbation theory to analyze the 1D model qualitatively in the limits when granule transport is either faster (Section 3), or slower (Section 4) than MT dynamics. In Section 5, we describe the numerical solutions of the 1D model equations. We report theoretical and experimental results on centering in 2D fragments in Section 6 and conclude with a discussion of the results and their biological implications in Section 7.

The influence of Lee Segel's work on mathematical modeling in cell biology, in particular on our modeling work reported here, is tremendous. Lee was one of the pioneers applying mathematics to cell biology in his now classical work on bacterial chemotaxis (Keller and Segel, 1971). He introduced the powerful idea of mathematical instability as a quantitative criterium for the onset of aggregation (Keller and Segel, 1970). He was one of the first researchers to recognize the role of non-local mechanisms in biology and to adapt integro-differential equations for mathematical modeling of these effects (Jager and Segel, 1992). Above all, Lee tirelessly and successfully promoted the art of scaling, nondimensionalization, qualitative and perturbation analysis of model equations (Segel, 1972; Lin and Segel, 1988), was ahead of his time in emphasizing attention to experimental details, and set a gold standard for research in mathematical biology.

2. Model assumptions and equations

Our model is based on the following properties of granules and MTs known from experiment (Rodionov and Borisy, 1997; Vorobjev et al., 2001; Cytrynbaum et al., 2004; Malikov et al., 2005):

1. MTs are straight and immotile.
2. MTs are nucleated both on pigment granules and in a spontaneous (granule-independent) manner at random locations in the cytoplasm with constant rates, with the majority nucleated on the granules.
3. Nascent MTs grow in random directions at a constant rate on the order of $0.1\,\mu$m/s by elongation at the plus ends, which stabilize when they reach the cell cortex.
4. Minus ends of nascent MTs remain stable for tens of seconds to a few minutes.
5. After a minus end is destabilized, the MT shortens at the minus ends with constant rate that is equal to the rate of plus-end growth.
6. Pigment granules are either detached from the MTs and static, or attached to a MT and move to the its minus end with a constant velocity on the order of $1\,\mu$m/s. The detachment rate is constant, while the attachment rate is proportional to local density of the MTs.

Qualitatively, the self-organization and centering phenomena can be explained as follows (Fig. 1A–D). The granules aggregate to the minus ends of existent MTs

and start to nucleate new MTs. The minus ends of these nascent MTs are stable for a while, so local mini-asters emerge. Then, when the plus ends of MTs recently nucleated in one granule-cluster reach other neighboring clusters, granules from those neighboring clusters are "stolen" by the former cluster. This leads to a merging of clusters, and eventually to the formation of a single granule aggregate with a single associated aster. If this aggregate is closer to the edge of the fragment than to its center, more spontaneously nucleated MTs would nucleate on the side of the aggregate away from the nearest edge as the rate of spontaneous MT nucleation per unit of cytoplasmic area is assumed to be constant across the cytoplasm. This asymmetry of spontaneous MT nucleation leads to a bias in the transport of pigment granules in the aggregate and directs their movement away from the cut edge. When the aggregate reaches the center of the fragment, the cytoplasmic area and thus the probability of MT nucleation on all sides of the aggregate becomes equal, keeping the aggregate in the center, equidistant from the cell margins. Note that there is a trade-off between the rate of centering generated by this mechanism and the width of the aggregate; more spontaneously nucleated MTs speed up centering but also counteract the aggregating influence of granule-nucleated MTs by pulling aggregated granules outward.

This explanation is supported by microscopy observations. In order to examine which quantitative features of motor and MT dynamics are essential for this behavior, we translate the assumptions into equations and analyze them. For simplicity, we introduce a one-dimensional system of equations which is applicable to a narrow long fragment. We discuss the realistic two-dimensional situation in Section 5.

We model the MTs and granules deterministically on the 1-D domain $-L < x < L$. We assume that there are sufficiently many MTs and granules that it is appropriate to keep track of them in terms of local densities. The MTs can be separated into two dynamic sub-populations characterized by opposite orientations. Each population is described by the dynamic densities of the plus ends ($p_{r,l}(x)$), static minus ends ($s_{r,l}(x)$) and shrinking minus ends ($m_{r,l}(x)$). The index r (l) stands for the right- (left-) oriented MTs, which have their minus ends to the right (left) of their plus ends. This notation is chosen because the pigment granules slide to the right (left) on right- (left-) oriented MTs. Another important characteristic of the MTs is the density $N_{r,l}(x)$ defined as the number of MTs (expressed as a density) passing through the cross-section of the fragment at coordinate x. The granules can be described by three densities—those gliding to the right (g_r) and left (g_l) with speed v_g on the right- and left-oriented MTs, respectively, and the density of static granules (g_s) dissociated from the MTs. The static granules associate with the right- (left-)oriented MTs with rates proportional to the local polymer densities of the respective fibers, $k_{on} N_{r,l}(x)$.

The equations governing the MT and granule dynamics are summarized by:

$$\frac{\partial p_{r,l}}{\partial t} = \pm v_p \frac{\partial p_{r,l}}{\partial x} + (\delta_0 + \delta_1 g), \quad \frac{\partial m_{r,l}}{\partial t} = \pm v_p \frac{\partial m_{r,l}}{\partial x} + \Gamma s_{r,l},$$

$$\frac{\partial s_{r,l}}{\partial t} = (\delta_0 + \delta_1 g) - \Gamma s_{r,l}, \quad g = g_r + g_l + g_s,$$

$$\frac{\partial g_{r,l}}{\partial t} = -k_{off}g_{r,l} + k_{on}N_{r,l}g_s \mp v_g\frac{\partial g_{r,l}}{\partial x}, \quad \frac{\partial g_s}{\partial t} = k_{off}(g_l + g_r) - k_{on}(N_r + N_l)g_s,$$

$$N_l(x) = \int_{-L}^{x}[s_l(y) + m_l(y) - p_l(y)]\,dy, \tag{1}$$

$$N_r(x) = \int_{x}^{L}[s_r(y) + m_r(y) - p_r(y)]\,dy. \tag{2}$$

The terms containing spatial derivatives in the right hand sides describe the advection of (growing) plus and (shrinking) minus ends at rate v_p, and of the granules at rate v_g. The terms $(\delta_0 + \delta_1 g)$ describe spontaneous and granule-based nucleation with rates δ_0 and $\delta_1 g$, respectively. The terms $\pm\Gamma s_{r,l}$ account for the destabilization of the static minus ends. The granules dissociate from the MTs with a constant rate k_{off} and attach with rates proportional to the rate k_{on} and the corresponding MT densities ($N_{r,l}(x)$). The expression for N_l is derived from the fact that the left-oriented MT density at x is equal to the number of fibers passing through the coordinate x, which can be found as the number of the minus ends to the left of x less the number of plus ends to the left of x. N_r is derived similarly. Equations (1) and (2) introduce nonlocality to the model, rendering it remarkably nontrivial.

Note that by tracking MT plus and minus end densities instead of MT densities, there is some ambiguity as to the exact structure of the MT network. In particular, this approach cannot distinguish between a single MT spanning the entire fragment from two parallel MTs arranged minus to plus end that together span the fragment. This ambiguity is not significant in the limit of rapid granule detachment, as assumed throughout our analysis, because, in this limit, granules rarely travel along a single MT from their attachment point all the way to the minus ends.

No boundary conditions are needed for the static minus end and granule densities. The natural boundary conditions for the other densities are:

$$p_r(L) = 0, \quad m_r(L) = 0, \quad p_l(-L) = 0,$$
$$m_l(-L) = 0, \quad g_r(-L) = 0, \quad g_l(L) = 0.$$

We choose half the size of the fragment, L, as the length scale, and the treadmilling rate, v_p, as the velocity scale so that the time scale is L/v_p. We choose the (uniform) density of pigment in the untreated fragment, $\bar{g}$, as the scale for granule density because the total number of granules is conserved. The characteristic scales of MT end densities are determined by the product of the characteristic nucleation rate and the characteristic time for a MT to treadmill across the fragment: $\bar{p}, \bar{m}, \bar{s} = \delta_1\bar{g}L/v_p$.

Using these scales, we arrive at the following non-dimensional form of the model equations:

$$\frac{\partial p_{r,l}}{\partial t} = \pm\frac{\partial p_{r,l}}{\partial x} + (\Delta + g), \quad \frac{\partial m_{r,l}}{\partial t} = \pm\frac{\partial m_{r,l}}{\partial x} + \gamma s_{r,l}, \tag{3}$$

$$\frac{\partial s_{r,l}}{\partial t} = (\Delta + g) - \gamma s_{r,l}, \, g = g_r + g_l + g_s, \tag{4}$$

$$\epsilon \frac{\partial g_{r,l}}{\partial t} = -k_1 g_{r,l} + k_2 N_{r,l} g_s \mp \frac{\partial g_{r,l}}{\partial x}, \quad \epsilon \frac{\partial g_s}{\partial t} = k_1 (g_l + g_r) - k_2 (N_r + N_l) g_s, \tag{5}$$

$$N_l(x) = \int_{-1}^{x} [s_l(y) + m_l(y) - p_l(y)] \, dy, \tag{6}$$

$$N_r(x) = \int_{x}^{1} [s_r(y) + m_r(y) - p_r(y)] \, dy, \tag{7}$$

with parameters defined as

$$\gamma = \Gamma L / v_p, \quad \Delta = \delta_0 / \delta_1 \bar{g},$$
$$\epsilon = v_p / v_g, \quad k_1 = k_{off} L / v_g, \quad k_2 = k_{on} L^3 \delta_1 \bar{g} / (v_g v_p), \tag{8}$$

and boundary conditons

$$p_r(1) = m_r(1) = p_l(-1) = m_l(-1) = g_r(-1) = g_l(1) = 0. \tag{9}$$

To avoid introducing confusing notation, here we use the same notation for both dimensional and non-dimensional variables.

The behavior of the model depends crucially on the five non-dimensional combinations of parameters given in (8). Two of them, $\epsilon \sim 0.1$ and $\Delta \sim 0.1$ are small (treadmilling is much slower than the motor transport and spontaneous nucleation is much slower than that on granules, respectively), while the other three γ, k_1, k_2 are hard to estimate from the experimental data. We deal with this situation by considering two different limiting cases that are feasible biologically and susceptible to asymptotic analysis. Other realistic regions of parameter space are explored numerically here and in (Cytrynbaum et al., 2004; Malikov et al., 2005).

3. Asymptotic analysis: Granule transport is faster than MT dynamics (1D)

In this section, we consider the case when $k_2 \gg k_1 \gg \epsilon^{-1}$ and $\Delta / \epsilon \ll \gamma \ll 1$: the granules attach to MTs faster than detach, both attachment and detachment are very rapid, the minus ends remain static for a time longer than needed for treadmilling across the fragment, and the MT spontaneous nucleation rate is very small. Using the notations $g = g_l + g_r + g_s$ and $h = g_l - g_r$ and adding and subtracting the equations in (5) for g_l, g_r, we obtain:

$$\epsilon \frac{\partial g}{\partial t} = \frac{\partial h}{\partial x}, \quad \epsilon \frac{\partial h}{\partial t} = \frac{\partial}{\partial x}(g_l + g_r) - k_1 h + k_2 (N_l - N_r) g_s. \tag{10}$$

Because $k_1, k_2 \gg \epsilon$, Eq. (5) for g_s is always in a pseudo-steady state relative to g_l, g_r, so $g_s \approx (k_1 / k_2)(g_l + g_r) / (N_r + N_l)$. Substituting this expression into the

equation for h, we find:

$$\epsilon \frac{\partial h}{\partial t} \approx \frac{\partial}{\partial x}(g - g_s) - k_1 h + k_1 \frac{N_l - N_r}{N_r + N_l}(g - g_s). \tag{11}$$

In the limit $k_2 \gg k_1$, g_s is small relative to g and the last equation reduces to:

$$\epsilon \frac{\partial h}{\partial t} \approx \frac{\partial g}{\partial x} - k_1 h + k_1 \frac{N_l - N_r}{N_r + N_l} g. \tag{12}$$

Taking time derivatives of the equation for g and spatial derivatives of this last equation for h, we can eliminate the variable h leaving the following equation for the variable g:

$$\frac{\epsilon^2}{k_1} \frac{\partial^2 g}{\partial t^2} + \epsilon \frac{\partial g}{\partial t} \approx \frac{1}{k_1} \frac{\partial^2 g}{\partial x^2} + \frac{\partial}{\partial x} \left(\frac{N_l - N_r}{N_r + N_l} g \right). \tag{13}$$

Finally, because $\epsilon^2/k_1 \ll 1$ and $1/k_1 \ll \epsilon$, we obtain heuristically the advection equation:

$$\frac{\partial g}{\partial t} \approx -\frac{1}{\epsilon} \frac{\partial}{\partial x}(Vg), \quad V = \frac{N_r - N_l}{N_r + N_l}. \tag{14}$$

The advection term in this equation has the following meaning: as granules come on and off quickly, they essentially sample the local MT population. Thus, their velocity is given by the difference between the probability of attaching to a left mover, $N_l/(N_r + N_l)$, and that of attaching to a right mover, $N_r/(N_r + N_l)$. In the limit $\gamma \ll 1$, Eqs. (3) and (4) indicate that $s_{r,l} \gg p_{r,l}, m_{r,l}$: most of the MT ends inside the fragment are static, because the treadmilling time is shorter than the minus end destabilization time. In addition, by the definitions of $N_r(x)$ and $N_l(x)$ given in (6) and (7), $N_r(x)$ and $N_l(x)$ are decreasing and increasing, respectively, with the boundary conditions $N_r(1) = 0$, $N_l(-1) = 0$. Thus, the effective velocity $V(x)$ has a single zero, is positive at the left and negative at the right: $V(x_0) = 0$; $V(x) > 0$ at $x < x_0$; $V(x) < 0$ at $x > x_0$. This means that on the fast time scale $t \sim O(\epsilon)$ the granules aggregate to a single peak at x_0: $g(x,t) \approx 2\delta(x - x_0)$. Then, on the slow time scale $t \sim O(1/\gamma)$ the MT density equilibrates to the quasi-steady-state determined by the granule density: $s_r \approx s_l \approx (\Delta + g(x))/\gamma = (\Delta + 2\delta(x - x_0))/\gamma$. Integrating, retaining linear terms with respect to Δ and neglecting smaller terms, we obtain the formula for the effective granule velocity:

$$V(x) \approx (1 - \Delta) \cdot \text{sign}(x_0 - x) - \Delta x, \tag{15}$$

where $\text{sign}(\cdot)$ is the signum function.

The first term in (15) corresponds to the strong self-aggregation of the granules to *arbitrary* location x_0. The small second term can be interpreted as the very slow velocity field $-(\Delta/\epsilon)x$, where x is the distance from the granules' aggregate to the center. Qualitatively, this interpretation is justified by the hierarchy of the time

scales: on the fast time scale $t \sim O(\epsilon)$ the granules aggregate to the delta-like peak at the location determined by the initial MT distribution, then on the slow time scale $t \sim O(1/\gamma)$ the MT distribution re-arranges into an aster with the center at the granules' peak, and finally on the very slow time scale $\epsilon/\Delta \gg 1/\gamma \gg \epsilon$ the peak together with the aster's focal point drifts to the center.

The asymptotic analysis predicts, most importantly, that the centering is only possible if there are spontaneously nucleated MTs, $\Delta > 0$, which is the main feature of the qualitative model that cannot yet be tested experimentally. Second, the model predicts that the granule aggregate approaches the center exponentially, with a decreasing rate:

$$\mathrm{d}x_0/\mathrm{d}t = -\Delta/\epsilon x_0, \quad x_0 = x_0(0)\mathrm{e}^{-t/T}, \qquad T = \frac{\epsilon}{\Delta}, \tag{16}$$

which is in agreement with the previously observed exponential approach to the center, and 5–10 min centering time (Rodionov and Borisy, 1997; Malikov et al., 2005), recalling that $\epsilon \sim \Delta \sim 0.1$ and the time scale was given by $L/v_p \sim (20–40\,\mu\mathrm{m})/(4\,\mu\mathrm{m/min}) = 5{-}10\,\mathrm{min}$.

4. Asymptotic analysis: Granule transport is slower than MT dynamics (1D)

To strengthen the results of the previous section, we consider another limiting case: if the rate of attachment of the granules to MT is very small, $k_2 \ll \epsilon\gamma^2 k_1$ then the MT density adjusts fast to a quasi-steady-state determined by the slowly changing granule density (justified below). As above, we assume that $\gamma \ll 1$, so, again, most of the MT ends inside the fragment are static minus ends. In the quasi-steady-state, $s_\mathrm{r} \approx s_\mathrm{l} \approx (\Delta + g(x))/\gamma$. Substituting these expressions into the equations for the MT densities ((6) and (7)) and using the boundary conditions (9), we obtain:

$$N_\mathrm{l} \approx \frac{\Delta}{\gamma}(x+1) + \frac{1}{\gamma}\int_{-1}^{x} g(y)\,\mathrm{d}y, \quad N_\mathrm{r}(x) \approx \frac{\Delta}{\gamma}(1-x) + \frac{1}{\gamma}\int_{x}^{1} g(y)\,\mathrm{d}y. \tag{17}$$

Thus, the average MT density is of the order $1/\gamma$, and in the limit $k_2/\gamma \ll k_1$, the detachment rate is much greater than the net rate of attachment, so most of the granules are static. Corresponding re-scaling of the moving granule densities by the small factor $k_2/(\gamma k_1)$ in Eq. (5) demonstrates that the temporal and spatial derivative terms in these equations can be neglected in comparison with the algebraic terms, and $g_{\mathrm{r,l}} \approx k_2 N_{\mathrm{r,l}} g_\mathrm{s}/k_1 \approx k_2 N_{\mathrm{r,l}} g/k_1$. Adding all three Eq. (5), we obtain the equation $\epsilon \partial g/\partial t = \partial/\partial x(g_\mathrm{l} - g_\mathrm{r})$, and substituting the approximate expressions for $g_{\mathrm{r,l}}$, we arrive at the approximate equation for the slow advection of the total granule density:

$$\frac{\partial g}{\partial t} \approx -\frac{k_2}{\epsilon k_1}\frac{\partial}{\partial x}\left([N_\mathrm{r} - N_\mathrm{l}]g\right). \tag{18}$$

Finally, substituting (17) into (18), we obtain the closed approximation for the granule density at the slow time scale:

$$\frac{\partial g}{\partial t} \approx -\frac{\partial}{\partial x}(V(x)g), \quad V(x) \approx \frac{k_2}{\epsilon k_1 \gamma}\left(-2\Delta x + \left[\int_x^1 g(y)\,\mathrm{d}y - \int_{-1}^x g(y)\,\mathrm{d}y\right]\right).$$

(19)

This equation demonstrates that the characteristic time scale of the granule dynamics, $\epsilon k_1 \gamma / k_2$, is much greater than that of the MT dynamics, $1/\gamma$ if the inequality $k_2 \ll \epsilon \gamma^2 k_1$ is valid.

In the case $\Delta = 0$, the velocity field $V(x)$ given by (19) advects the granules toward the center of the granule distribution, since, at each x, $V(x)$ is positive (negative) if there are more granules located to the right (left) of x. Therefore, the granules aggregate and we expect that their density converges to a peak. Indeed, Grindrod (1991) showed that at $\Delta = 0$, the solution of Eq. (19) converges to the delta-function: $g(x,t) \to 2\delta(x - x_0)$, where x_0 is the arbitrary position of the peak. (In fact, the next orders of magnitude of the perturbation theory predict the centering even in the case $\Delta = 0$, but on an astronomically long time scale.)

At small, yet finite, values of Δ, Eq. (19) predicts that the position of the granule aggregate would slowly drift toward the center of the aggregate with the centering velocity $-2\Delta k_2 x_0 / (\epsilon k_1 \gamma)$. This formula, similarly to the result of the previous section, predicts that the granule aggregate approach the center exponentially, with the slowing rate, and that the spontaneously nucleated MTs are crucial for the centering.

5. Numerical analysis of aggregation and centering (1D)

To further corroborate the results of the asymptotic analysis and to gain additional insight, we numerically solved the model equations in (3), (4), (6) and (7) for the MT densities. Rather than explicitly solving the equations in (5) governing the granule dynamics, we assumed that at each computational step the granule density is in a quasi-steady state characterized by the advection-diffusion equation

$$\frac{1}{k_1}\frac{\partial^2 g}{\partial x^2} - \frac{\partial}{\partial x}\left(\frac{N_r - N_l}{N_r + N_l}g\right) \approx 0,$$

(20)

which approximates Eq. (13) in the limiting case when $\epsilon \ll 1$, $k_1 \ll k_2$, $k_1 \ll 1/\epsilon$. Note that in this case, the granule dynamics are fast in comparison with the MT dynamics justifying the quasi-steady state approximations on a time scale slower than $\sim \epsilon$. Also, in this limit the model behavior does not depend on parameters ϵ, k_2. We solved Eqs. (3), (4), (6), (7) and (20) (the latter with no flux boundary condition) using the parameter values $k_1 = 20$, $\gamma = 1$ and varying parameter Δ from 0 to 3. To simulate realistic conditions in the nascent fragment, we assumed that initially

there were only MTs with their minus ends at the very left and plus ends at the
very right and constant granule density. The simulations were done on a desktop
computer using Matlab with the forward explicit methods (Euler for Eq. (4), up-
and down-wind for Eq. (3), centered difference for the integral of Eq. (20)) with
the time step small enough for numerical stability (Garcia, 2000).

The simulation results are shown in Fig. 2. Figure 2A and B illustrates that a
fully developed granule aggregate forms near the left edge of the fragment within
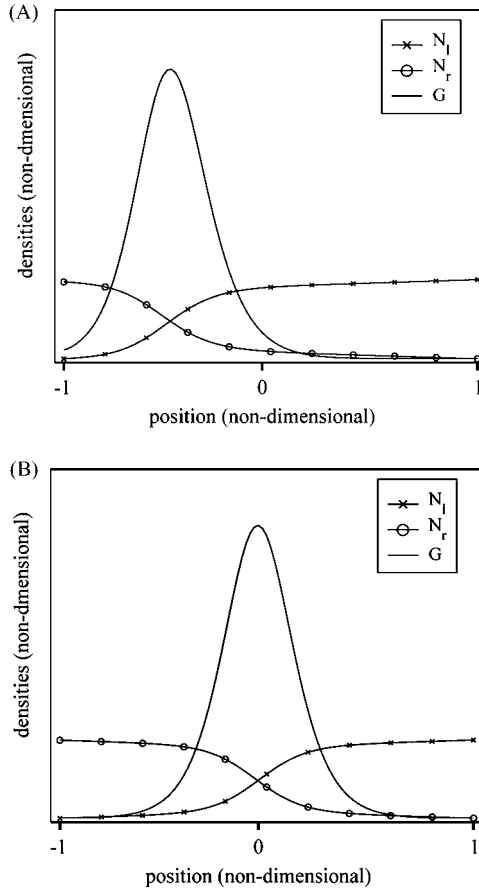
Fig. 2 (A–B) Computed total granule density (*solid*) and the densities of the left- and right-
oriented MTs ($\times$, $\circ$) are shown at 5 (A) and 50 (B) time units after the simulations started. This
simulation of the model equations with parameter values $\Delta = 0.2$, $\gamma = 1$ and $k_1 = 20$ demon-
strates that the granules rapidly aggregate to the single peak, the MTs organized into the aster
(A), and then the granule aggregate and the aster focal point slowly drifted toward the center
(B). (C) The characteristic time constant of the centering (*solid*) determined numerically is a de-
creasing function of the spontaneous nucleation rate, while the characteristic time of aggregation
(*dashed*) is insensitive to the spontaneous MT nucleation. Note that peak height and width were
both used as measures of the state of aggregation. We found good agreement between them so
only one is shown here. (D) The dispersion of the granules in the aggregate increases with Δ (ratio
of spontaneous nucleation granule-based nucleation).
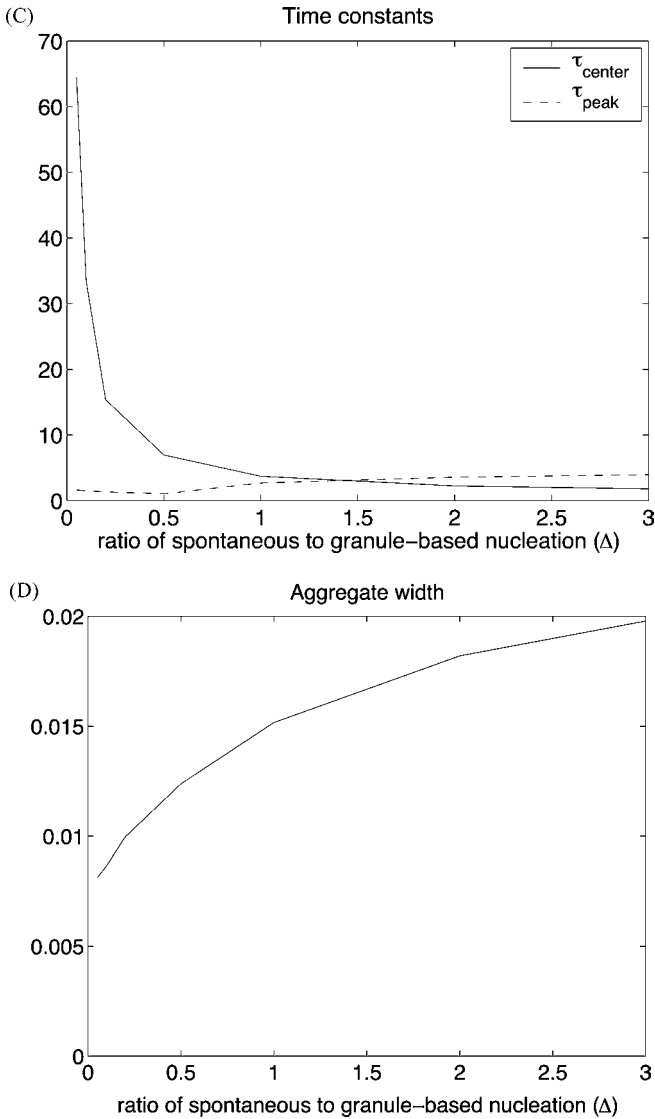
Fig. 2 Continued.

1–2 time units, and then this aggregate, together with its aster-like MT structure drifts slowly toward the center, in agreement with the analytical results. Figure 2C shows that the fast time scale of granule aggregation is relatively insensitive to the relative levels of granule-mediated to spontaneous nucleation, while the characteristic centering time is a decreasing function of the spontaneous nucleation rate. Figure 2D demonstrates that the granule aggregate becomes wider as the spontaneous nucleation rate increases. This result has the following important biological interpretation: the ratio of the spontaneous nucleation to nucleation on the

granules can be neither too small (in which case the centering would be too slow), nor too great (in which case the spontaneously nucleated MTs would overcome the focussing effect of the granule-nucleated MTs and disperse the aggregate).

6. Centering in 2D complex-shaped fragments

Asymptotic analysis of the last limiting case can be extended heuristically to the two-dimensional system leading to important novel predictions. A non-rigorous generalization, similar to that presented in Cytrynbaum et al. (2004), of the Eqs. (18) and (19) gives the following higher dimensional formulation:

$$\frac{\partial g}{\partial t} = -\nabla \cdot (\mathbf{V}(\mathbf{x})g), \quad \mathbf{V}(\mathbf{x}) = \frac{k_2}{\epsilon k_1} \int_0^{2\pi} N(\mathbf{x}, \theta) \mathbf{n}_\theta \, d\theta,$$

$$\mathbf{n}_\theta = \cos(\theta)\mathbf{i} + \sin(\theta)\mathbf{j},$$

where the MTs densities, $N_r(x)$ and $N_l(x)$ have been replaced by an angle dependent density $N(\mathbf{x}, \theta)$.

This equation can be interpreted as follows: the advection of granules at $\mathbf{x}$ is determined by the superposition of simultaneous movement along all MTs passing through $\mathbf{x}$; this can be thought of as a rapid sampling of the local MT network by rapid attachment and detachment of granules. To find the number of MTs passing through $\mathbf{x}$ and leading the granules in the direction $\mathbf{n}_\theta$, it is sufficient to integrate over all points visible from $\mathbf{x}$ (that is, the union of all points lying on line segments that connect $\mathbf{x}$ to the boundary to the fragment and that lie entirely inside the fragment). The number of MTs reaching $\mathbf{x}$ from a point $\mathbf{y}$ is determined by both the granule density at $\mathbf{y}$ (due to granule-based nucleation) and the spontaneous nucleation rate Δ. These MTs contribute to the motion of granules at $\mathbf{x}$ in the direction $\mathbf{y} - \mathbf{x}$. Thus,

$$\mathbf{V}(\mathbf{x}) = \frac{k_2}{\epsilon k_1 \gamma} \left(\int_{\mathbf{\Omega}(x)} g(\mathbf{y}) \frac{\mathbf{y} - \mathbf{x}}{|\mathbf{y} - \mathbf{x}|} \, d\mathbf{y} + \Delta \int_{\mathbf{\Omega}(x)} \frac{\mathbf{y} - \mathbf{x}}{|\mathbf{y} - \mathbf{x}|} \, d\mathbf{y} \right). \tag{21}$$

Here $\mathbf{\Omega}(x)$ is the area of the fragment *that is visible* from $\mathbf{x}$.

We argue that because the first term in (21) describes the advection of the granules in the approximate direction of the highest granule density, this term in simple-shaped fragments is responsible for the granule aggregation into a single peak, the position of which is arbitrary, similar to the 1D case. Then, also by analogy with the 1D case, the global velocity field established by spontaneously nucleated MTs that treadmill into the aggregate:

$$\mathbf{V}(\mathbf{x})_{\text{cent}} \sim \int_{\mathbf{\Omega}(x)} \frac{\mathbf{y} - \mathbf{x}}{|\mathbf{y} - \mathbf{x}|} \, d\mathbf{y}, \tag{22}$$

determines the slow drift of the pigment aggregate.
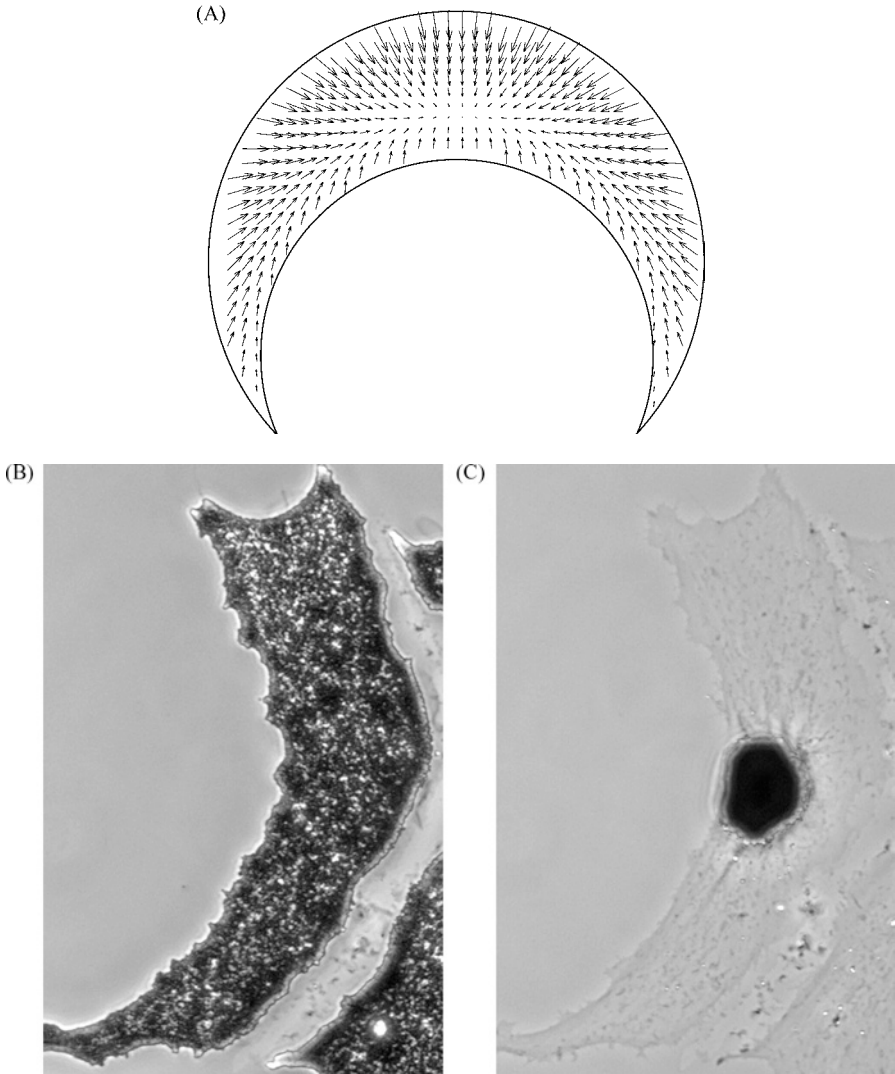
Fig. 3 The theoretical global velocity field established by the spontaneously nucleated MTs predicts that the granule aggregate centers closer to the concave boundary of the crescent-shaped fragment (A). The experiment confirms this prediction (B, C). The spatial and temporal scales and experimental methods are as described in Fig. 1.

We plotted this velocity field numerically (using a simple Matlab^{TM} code) for three complex-shaped fragments: crescent-like (Fig. 3A), bi-lobed (Fig. 4A), and a "wounded" disk (Fig. 5A). Experimental results are in striking agreement with the theory. In the crescent-like fragment, the velocity field converges to the globally stable single node that is closer to the concave boundary of the fragment. The reason is that many MTs originate at the bottom of the fragment
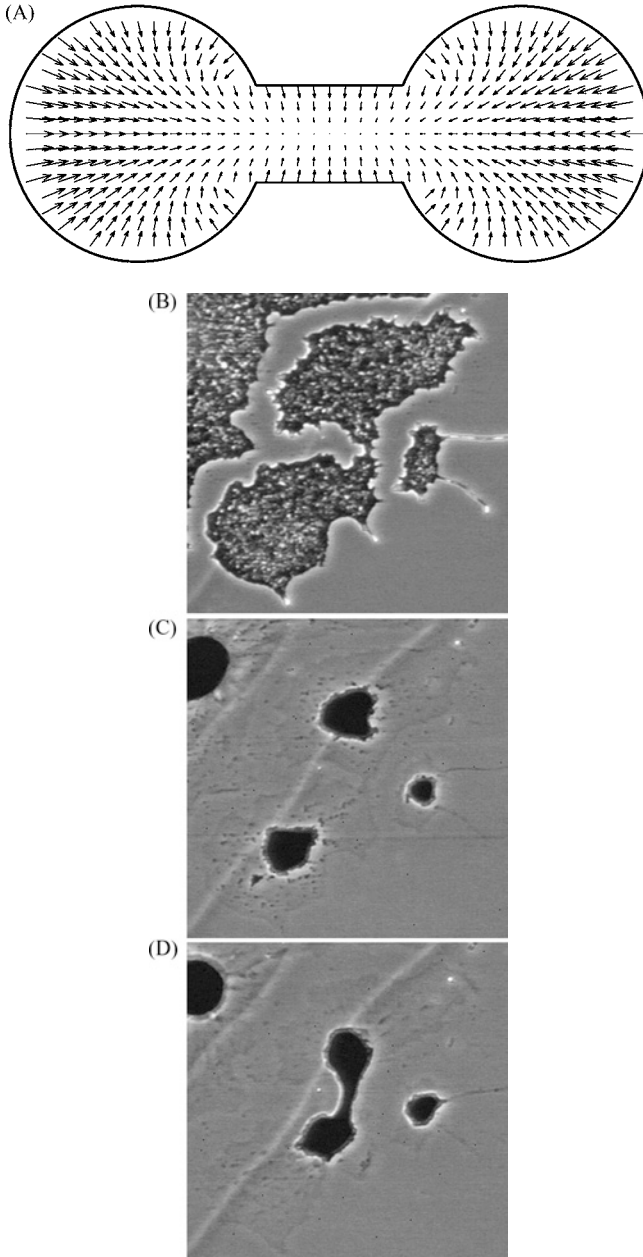
Fig. 4 The theoretical global velocity field established by the spontaneously nucleated MTs predicts that the granule aggregate centers to the midpoint of the neck in the bi-lobed fragment (A). The experiment confirms this prediction for the fragment of similar shape (B) demonstrating that in a few minutes two aggregates appear in the centers of the lobes (C) merging in the next 10 min in the corridor between the lobes (D). The spatial scales and experimental methods are as described in Fig. 1.

establishing the downward bias. The experimental result confirms this prediction (Fig. 3C).

Similarly, the model predicts aggregation to the center of the corridor between two lobes in the bi-lobed fragment (Fig. 4A). The experiment confirms this prediction (Fig. 4D). (Figs. 3B and 4B show the original geometries of the fragments as they are difficult to identify after aggregation.) Note that the corridor in the experimental fragment is so narrow that the granules "spill out" from it into the lobes. Curiously, before converging to the center, the granules aggregate first to the centers of the lobes (Fig. 4C). The model explains this phenomenon as follows: Initially, very few MTs pass through the corridor, so there is little communication between the lobes. Thus, self-organization proceeds in the lobes almost independently, according to the scenario for regularly shaped fragments. However, after two polar asters are organized in the adjacent lobes, there is an increased number of MTs transiently anchored by their minus ends in one of the granule aggregates extending through the corridor and passing through the other aggregate. These MTs establish tracks for granules transport, so that granule density in the corridor increases. This augments the nucleation of MTs with their minus ends in

(A)
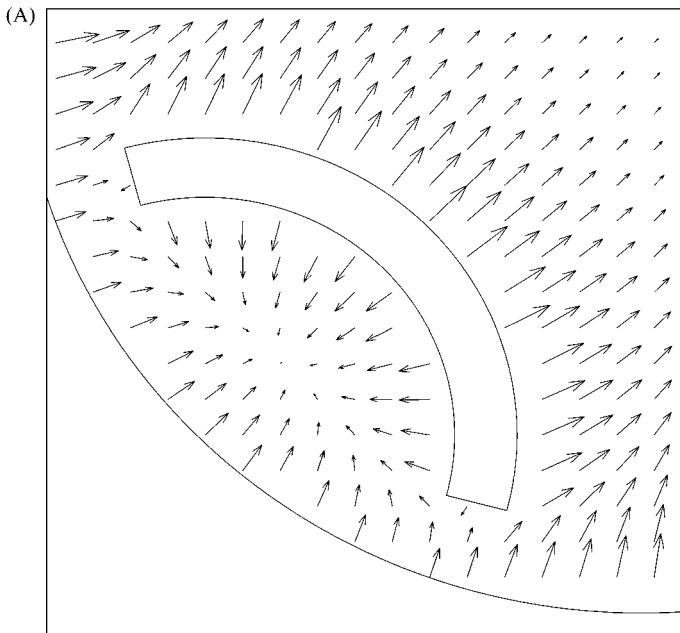
Fig. 5 The theoretical global velocity field established by the spontaneously nucleated MTs in the disc-like fragment with the curved "wound" near the edge of the disc (only a quarter of the disc is shown) predicts that most of the granules aggregate toward the center of the disc, while some of them aggregate into a local cluster "protected" from the global center by the wound. The experiment confirms this prediction for the fragment of a similar shape (B) demonstrating that in a few minutes two aggregates appear (C). Curiously, after tens of minutes, a *single bent* MT reaching from the global center into the area behind the wound (D) transports *all* granules into the bigger aggregate. The spatial scales and experimental methods are as described in Fig. 1.
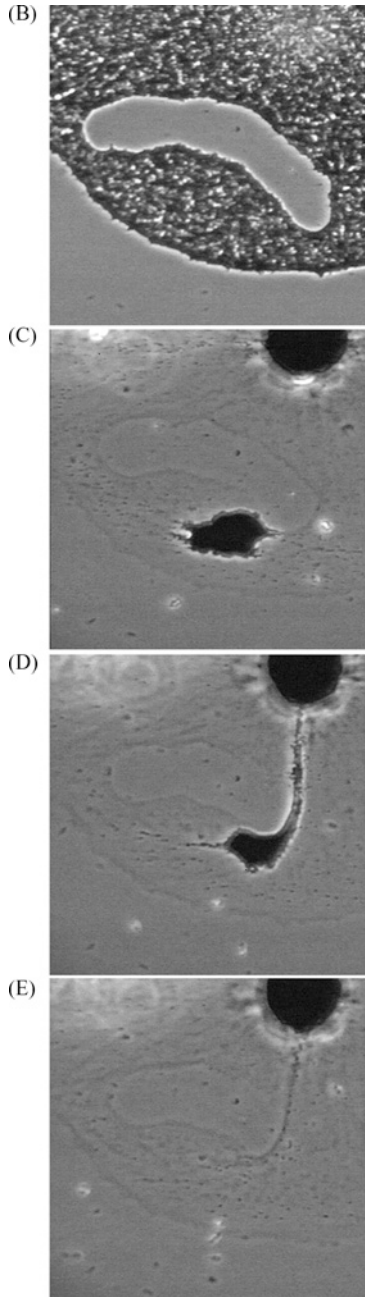
Fig. 5 Continued.

the corridor extending outward and thus passing through both granule aggregates. This accelerates directional granule traffic into the corridor further enhancing the formation of a polar MT aster in the corridor and depleting granules from the initial aggregates. This positive feedback loop leads to the final centered aggregation.

Finally, the model predicts *two* locally stable single nodes in the velocity field for the "wounded" disk-shaped fragment (Fig. 5A), because the wound screens out a small area near the boundary of the fragment. As expected, the experiment showed that two corresponding granule aggregates emerged in the predicted locations (Fig. 5B and C). However, astonishingly, a single *bent* MT extended from the bigger aggregate into the screened area (Fig. 5D) and established a track on which all granules from the smaller aggregate moved and merged with the main aggregate (Fig. 5E). This observations points out a model limitation: even small MT bending can on the long time scale perturb stability of the locally stable cytoskeleton patterns.

7. Discussion

In this paper, we showed that, while the self-organization and centering of MT asters depends on MT dynamics and the activity of dynein, it need not involve the application of forces nor MT transport. Instead, the pattern formation occurs through minus end directed transport of granules, nucleation of MTs on the granules and elsewhere in the cytoplasm and MT treadmilling. This novel *purely geometric* self-organization and centering mechanism relies on the minus-end transport/nucleation positive feedback and on sensing of cytoplasmic volume through spontaneous nucleation of MTs around the pigment aggregate. The model explains self-organization as a positive feedback loop based on the mutually enhancing processes of motor transport to MT minus ends leading to motor concentration and motor-mediated nucleation of the MT minus ends. The centering is due to the non-local geometric effect generated by spontaneously nucleated MTs which establish a global directional bias for the motors.

In order to test the model, we made theoretical predictions for pattern formation in the bi-lobed, crescent and "wounded" fragments and compared them with experimental observations. The semi-quantitative agreement between experiment and theory lends additional support to the model. Another model prediction is that changes of total MT nucleation rate do not significantly affect the centering rate, but the ratio of MTs nucleated locally on the pigment granules to those nucleated at the random sites in the cytoplasm is of critical importance. If the fraction of spontaneously nucleated MTs is too great, MT minus ends are no longer focussed and the radial organization was lost. If the fraction of spontaneously nucleated MTs is too small, the radial array is formed, but moves to the center too slowly. Therefore, in order for the radial MT array to form and relocate to the center, a delicate balance is essential between the rate of MT nucleation on the pigment granules and in the peripheral cytoplasm.

Mathematical analysis in this paper provides significant insight into the mechanisms of transport and polarization in the cell and is complementary to results of previous computational modeling. More rigorous mathematical investigation of our model, similar to that in (Kang et al., 2005), will lead to further understanding

of the pattern formation in polymer–motor systems. Also, the model can be extended in the future to more general self-organization phenomena in cytoskeleton.

References

Bray, D., 2002. Cell Movements. Garland, New York.

Burakov, A., Nadezhdina, E., Slepchenko, B., Rodionov, V., 2003. Centrosome positioning in interphase cells. J. Cell Biol. 162, 963–969.

Cytrynbaum, E., Rodionov, V., Mogilner, A., 2004. Computational model of dynein-dependent self-organization of microtubule asters. J. Cell Sci. 117, 1381–1397.

Garcia, A.L., 2000. Numerical Methods for Physics. Prentice Hall, Englewood Cliffs, NJ.

Grindrod, P., 1991. Patterns and Waves. Claredon Press, Oxford, UK.

Holzbaur, E.L., Vallee, R.B., 1994. Dyneins: molecular structure and cellular function. Annu. Rev. Cell Biol. 10, 339–372.

Jager, E., Segel, L.A., 1992. On the distribution of dominance in a population of interacting anonymous organisms. SIAM J. Appl. Math. 52, 1442–1468.

Kang, K., Kololkolnikov, T., Ward, M.J., 2005. The stability and dynamics of a spike in the one-dimensional Keller-Segel model. IMA J. Appl. Math. in press.

Keller, E.F., Segel, L.A., 1970. The initiation of slime mold aggregation viewed as an instability. J. Theor. Biol. 26, 399–415.

Keller, E.F., Segel, L.A., 1971. Model for chemotaxis. J. Theor. Biol. 30, 225–234.

Kellogg, D.R., Moritz, M., Alberts, B.M., 1994. The centrosome and cellular organization. Annu. Rev. Biochem. 63, 639–674.

Lin, C.C., Segel, L.A., 1988. Mathematics Applied to Deterministic Problems in the Natural Sciences. Macmillan Publishing Co., New York.

Malikov, V., Cytrynbaum, E.N., Kashina, A., Mogilner, A., Rodionov, V., 2005. Centering of a radial microtubule array by translocation along microtubules spontaneously nucleated in the cytoplasm. Nat. Cell Biol. 7, 1213–1218.

Maly, I.V., Borisy, G.G., 2002. Self-organization of treadmilling microtubules into a polar array. Trends Cell Biol. 12, 462–465.

Nascimento, A.A., Roland, J.T., Gelfand, V.I., 2003. Pigment cells: a model for the study of organelle transport. Annu. Rev. Cell Dev. Biol. 19, 469–491.

Nedelec, F.J., Surrey, T., Maggs, A.C., Leibler, S., 1997. Self-organization of microtubules and motors. Nature 389, 305–308.

Rodionov, V.I., Borisy, G.G., 1997. Self-centering activity of cytoplasm. Nature 386, 170–173.

Rodionov, V.I., Lim, S.-S., Gelfand, V.I., Borisy, G.G., 1994. Microtubule dynamics in fish melanophores. J. Cell Biol. 126, 1455–1464.

Segel, L.A., 1972. Simplification and Scaling. SIAM Review 14, Macmillan, New York, pp. 547–571.

Schiebel, E., 2000. Gamma–tubulin complexes: Binding to the centrosome, regulation and microtubule nucleation. Curr. Opin. Cell Biol. 12, 113–118.

Tran, P.T., Marsh, L., Doye, V., Inoue, S., Chang, F., 2001. A mechanism for nuclear positioning in fission yeast based on microtubule pushing. J. Cell Biol. 153, 397–411.

Verde, F., Berrez, J.M., Antony, C., Karsenti, E., 1991. Taxol-induced microtubule asters in mitotic extracts of Xenopus eggs: Requirement for phosphorylated factors and cytoplasmic dynein. J. Cell Biol. 112, 1177–1187.

Vorobjev, I., Malikov, V., Rodionov, V., 2001. Self-organization of a radial microtubule array by dynein-dependent nucleation of microtubules. Proc. Natl. Acad. Sci. USA 98, 10160–10165.